Progress of Large Size BaF_2:Y Crystals for Future HEP Experiments

Chen Hu[a], Liyuan Zhang[a], Ren-Yuan Zhu[a], Junfeng Chen[b], and Mingrong Zhang[c]

[a] High Energy Physics Laboratory, California Institute of Technology, Pasadena, CA 91125, USA

[b] Shanghai Institute of Ceramics, 1295 Dingxi Rd, Shanghai, 200050, China

[c] Beijing Glass Research Institute, 5 Xingguang Ave, Beijing, 101111, China

1. Introduction and Samples

Because of its ultrafast light with sub-ns decay time and suppressed slow scintillation yttrium doped barium fluoride (BaF_2:Y) crystals attract a broad interest in the HEP community pursuing ultrafast calorimetry, such as Mu2e-II. R&D continues to optimize yttrium doping uniformity and radiation hardness for BaF_2:Y crystals of large size. Fig. 1 shows long BaF_2:Y crystals with suppressed slow component grown by BGRI and SIC. Figs. 2 and 3 show respectively their longitudinal transmittance and light output as a function of integration time, measured at Caltech HEP crystal lab. 2020 samples show no impurity or defects induced absorption band, a consistent fast scintillation component (A0) of about 100 p.e./MeV and the fast/slow ratio (A0/A1 or F/S) of 0.64 and 1.1 respectively for the samples from BGRI and SIC.

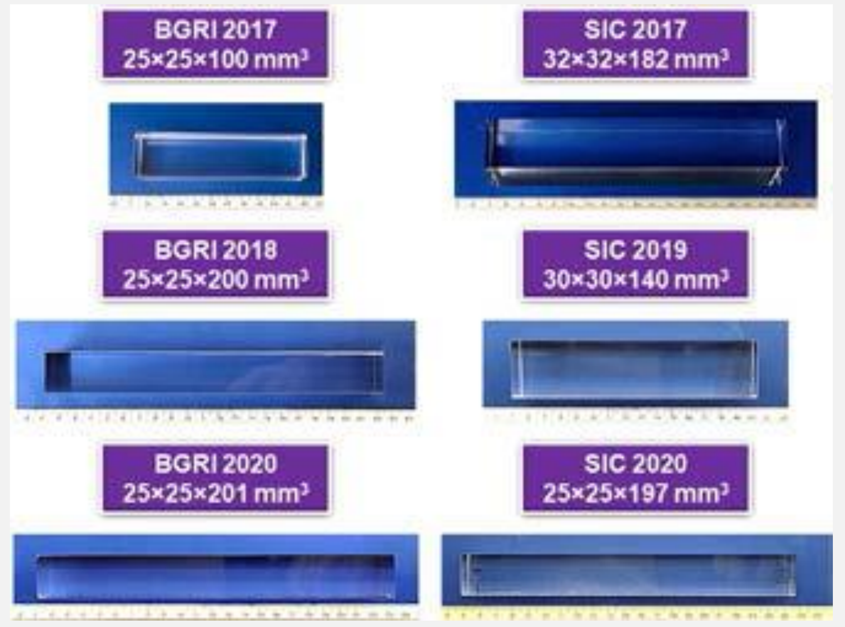

Fig. 1 Six long BaF2:Y crystals produced by BGRI (left) and SIC (right) from 2017 to 2020 for the Mu2e-II experiments.

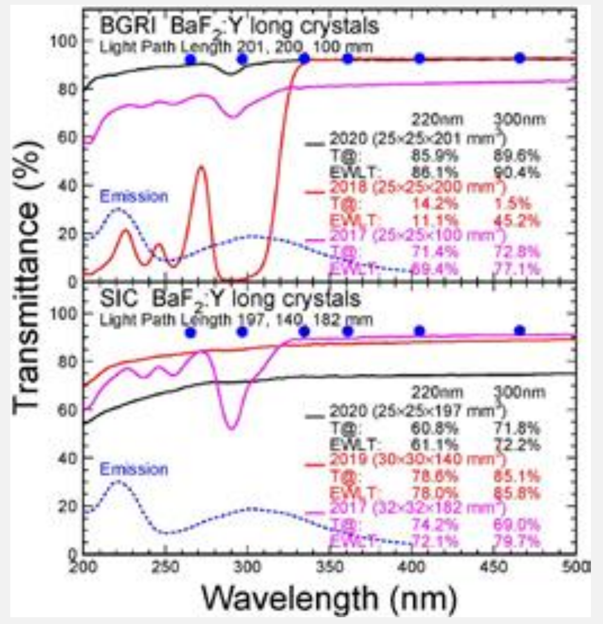

Fig. 2 Longitudinal transmittance for the 6 samples (solid lines) and the x-ray excited emission (blue dots).

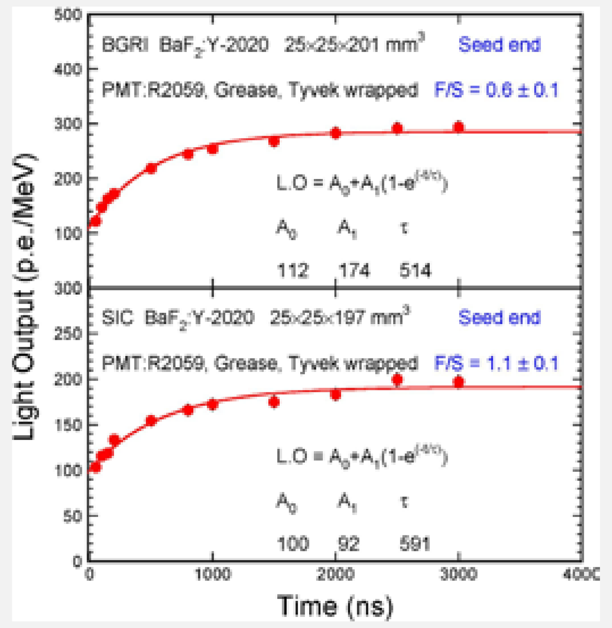

Fig. 3 light output is shown as a function of integration time for 2020 BGRI (top) and SIC (bottom) samples.

2. Radiation Induced Readout Noise and Damage

Fig. 4 shows a setup used to measure Gamma-ray induced photocurrent and readout noise (RIN) measured by an R2059 PMT via an air gap coupled to BaF_2:Y samples wrapped by Tyvek under 2 and 23 rad/h by ^{60}Co ɣ-rays. F is the radiation induced photoelectron number per second, normalized to the dose rate or neutron flux. RIN (σ) is the fluctuation of photoelectron number (Q) normalized to the light output (LO) in the readout gate for the BaF_2 sample. Figs. 5, 6 and 7 show the photocurrent history of two SIC BaF_2 samples, one BGRI BaF_2 sample and two BaF_2:Y samples from BGRI (top) and SIC (bottom) respectively under 23 rad/h. Significant reduced photocurrent was observed in BaF_2:Y samples.

$$F = \frac{\frac{Photocurrent}{Charge_{electron} \times Gain_{PMT}}}{Dose\ rate_{\gamma-ray}\ or\ Flux_{neutron}}$$

$$\sigma = \frac{\sqrt{Q}}{LO}\ \text{MeV}$$

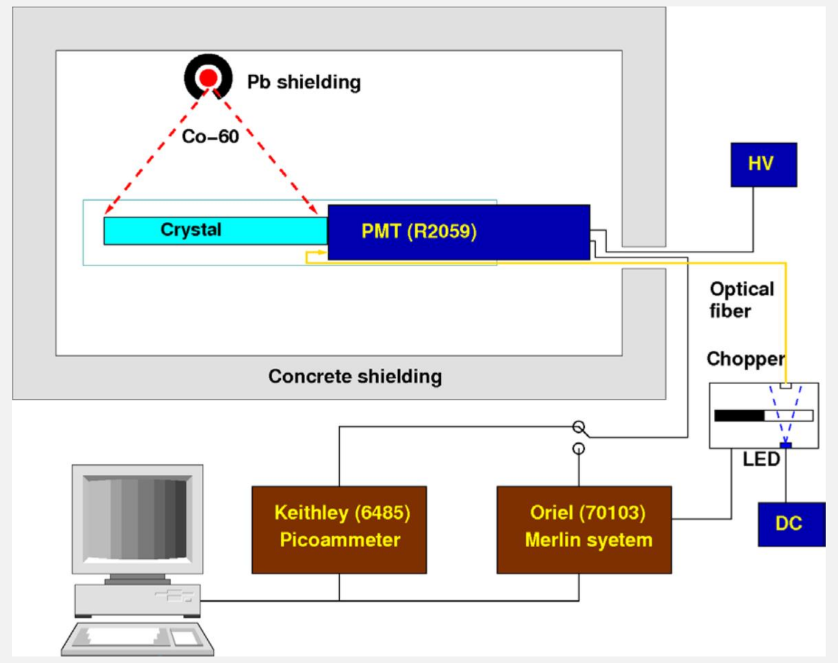

Fig. 4 A setup used to measure γ-ray induced photocurrent before, during and after irradiation for BaF_2 and BaF_2:Y samples.

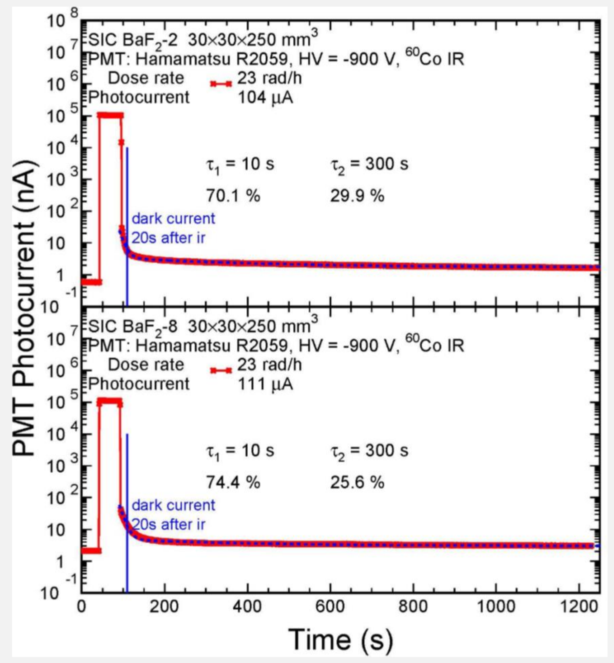

Fig. 5 Photocurrent measured by the Hamamatsu R2059 PMT for two SIC BaF_2 samples under 23 rad/h.

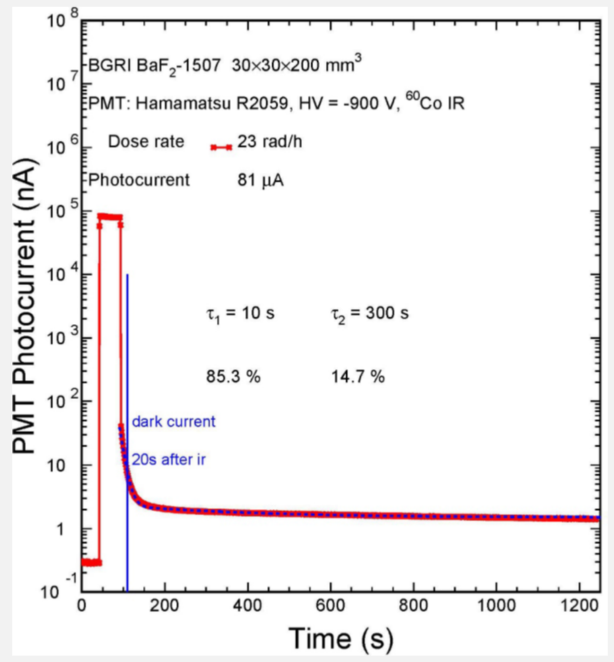

Fig. 6 Photocurrent measured by the Hamamatsu R2059 PMT for one BGRI BaF_2 samples under 23 rad/h.

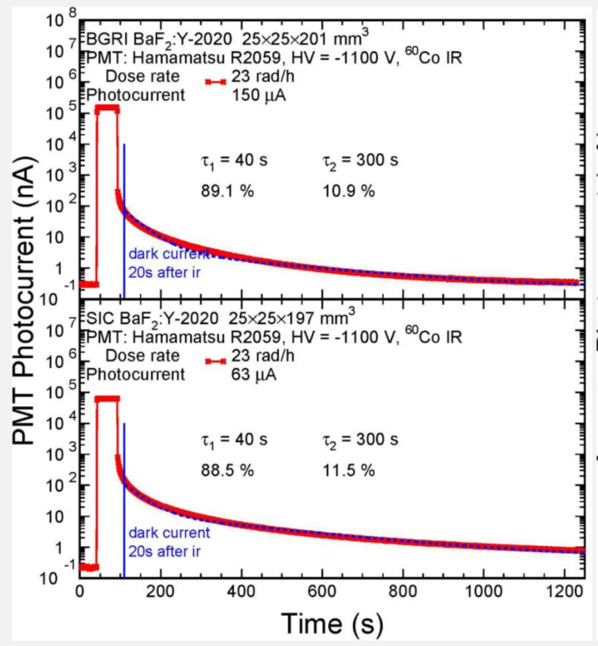

Fig. 7 Photocurrent measured by the Hamamatsu R2059 PMT for BGRI (top) and SIC (bottom) BaF_2:Y samples under 23 rad/h.

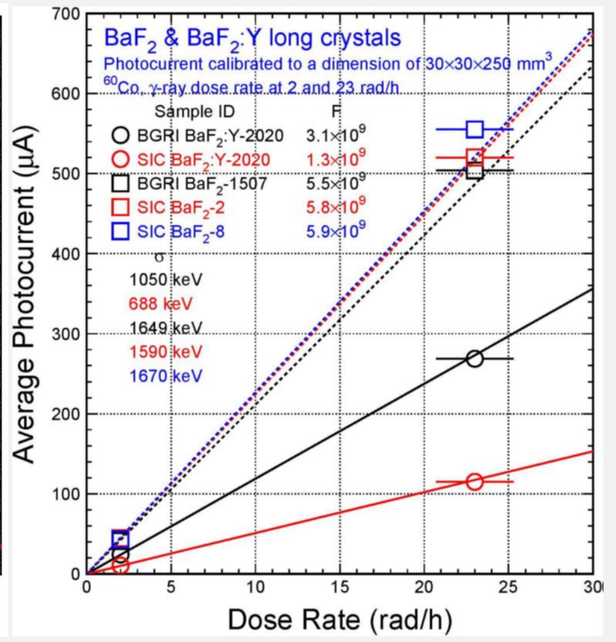

Fig. 8 Photocurrent is shown as a function of the dose rate for 2 BaF_2:Y and 3 BaF_2 samples under 2 and 23 rad/h.

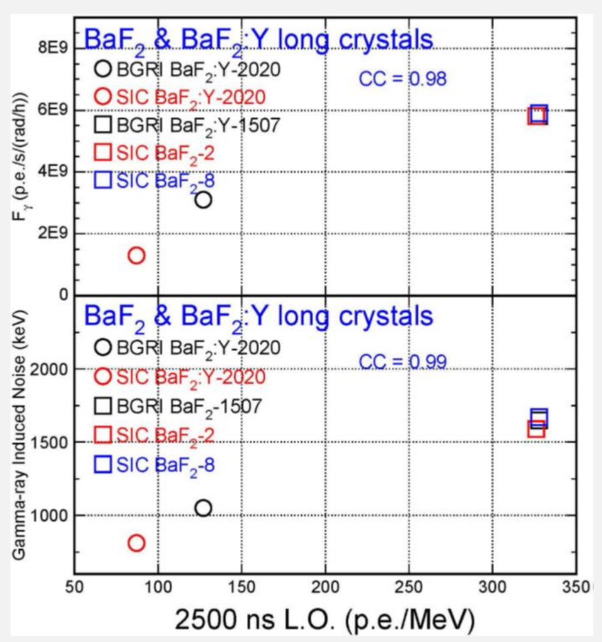

Fig. 9 Gamma induced photocurrent (top) and readout noise (bottom) are shown as a function of the light output in 2,500 ns gate.

Fig. 8 shows the average PMT photocurrent during irradiation as a function of the dose rate for two BaF_2:Y and three BaF_2 samples under 2 and 23 rad/h. An excellent linearity was observed between the γ-ray induced photocurrent and the dose rate. It is clear that yttrium doping in BaF_2 reduces the γ-ray induced photocurrent significantly. Fig. 9 shows that γ-ray induced photocurrent (top) and readout noise (bottom) are highly correlated to the light output in 2,500 ns gate, or the slow component, but not the fast component. Table I summarizes the F factor and the RIN (σ) values. Figs. 10 and 11 show longitudinal transmittance (LT) before, after 10, 100 and 1,000 krad, and 20 days' recovery for 2017 BaF_2:Y samples from BGRI and SIC respectively at room temperature, confirming no recovery in transmittance damage. Fig. 12 shows normalized light output (top) and EWLT as a function of the integrated dose. We note that crystal quality is diverse at this stage of R&D, so needs to be improved.

Table I: A Summary of photocurrent, $F_ɣ$ factor and gamma-ray induced readout noise for 2 BaF_2:Y and 3 BaF_2 samples

Crystal ID	L.O. corrected to air gap (p.e./MeV)*		F/S	Dose rate (rad/h)	Dark cur. before irrad. (nA)	Photo cur. (μA)	Dark cur. 20s after irrad. (nA)	Dark cur after 20s/Photo cur. (×10⁻⁴)	Dark cur. after 1000s –before irrad. (nA)	F (p.e./s/(rad/h))	σ (keV)
	50 ns	2500 ns									
BGRI BaF_2:Y-2020	53	127	0.64	2	0.5	24	34	14	0.05	3.1×10^9	1050
				23	0.5	269	122	4.5	0.22		
SIC BaF_2:Y-2020	45	87	1.08	2	0.4	10	30	29	0.03	1.3×10^9	810
				23	0.4	115	245	21	1.0		
BGRI BaF_2-1507	46	328	0.10	2	0.8	41	5.7	1.4	1.6	5.8×10^9	1650
				23	1.8	504	43	0.9	7.5		
SIC BaF_2-2	48	326	0.10	2	6.0	45	10	2.1	0.92	5.8×10^9	1590
				23	3.0	520	24	0.5	5.9		
SIC BaF_2-8	46	328	0.09	2	2.0	43	10	2.3	1.1	5.9×10^9	1670
				23	11	555	63	1.1	5.3		

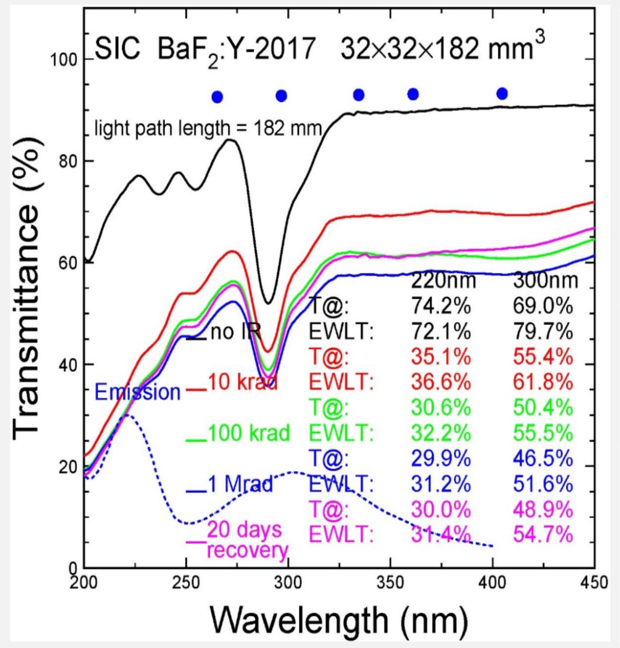

Fig. 10 Transmittance of the SIC 2017 BaF_2:Y sample after 10, 100 & 1,000 krad, and after 20 days' recovery.

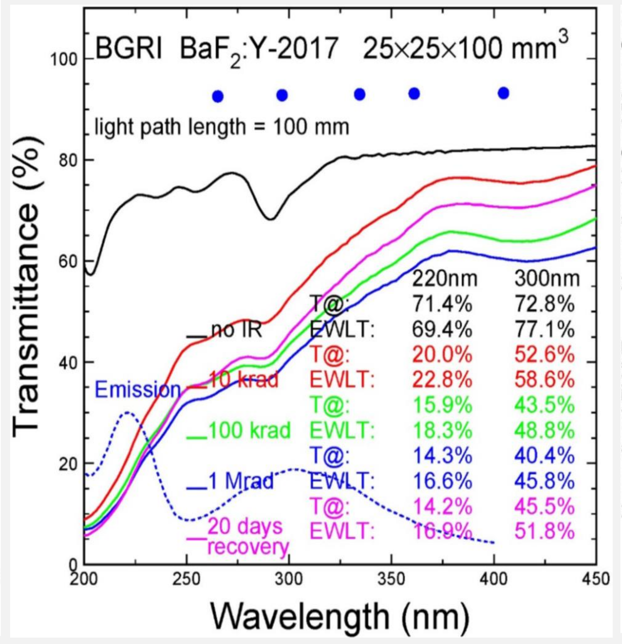

Fig. 11 Transmittance of the BGRI 2017 BaF_2:Y after 10, 100 and 1,000 krad, and after 20 days' recovery.

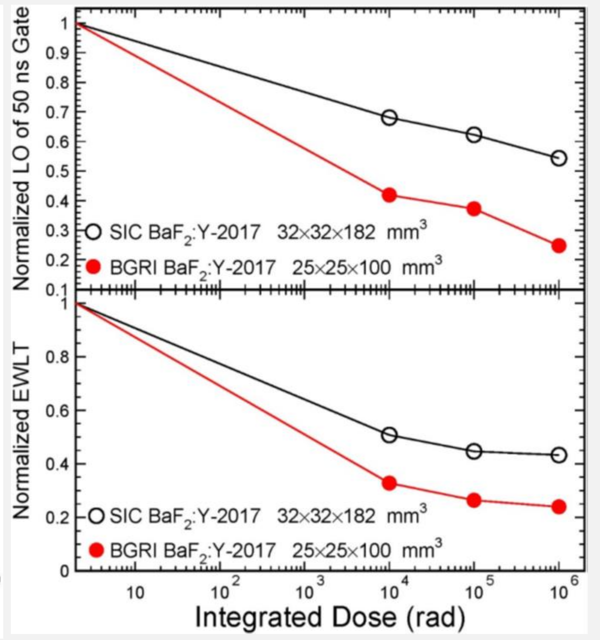

Fig. 12 LO in 50 ns gate (top) and EWLT (bottom) as a function of γ-ray dose for two 2017 BaF_2:Y samples.

3. VUV Photodetectors for BaF_2 Readout

RIN:ɣ is found highly correlated to the light output in 2.5 μs gate, but not 50 ns gate, indicating the dominance of the slow scintillation component. In addition to the selective doping in BaF_2, R&D has also been carried out for solar-blind VUV photodetectors sensitive to the fast but not the slow component. QE or PDE were measured for four Hamamatsu R2059 PMT, a Photek solar-blind photocathode, a Hamamatsu VUV MPPC and a few FBK VUV SiPMs with integrated filter. Table II summarizes emission weighted QE/PDE for the fast component and the corresponding F and RIN:ɣ values for 4 VUV photodetectors for four BaF_2 and BaF_2:Y samples. The results show that both yttrium doping and solar blind photodetector are needed to reduce the RIN:ɣ to less than 0.6 MeV.

Table II: A Summary of 4 VUV photodetectors for BaF_2 and BaF_2:Y readout.

Photodetector	$EWQE/PDE_{fast}$ (%)	EWQE/PDE (%)	LO(50 ns) p.e./MeV	F	RIN:ɣ (keV)
BGRI BaF_2:Y-2020					
Hamamatsu R2059 PMT	15.2	18.7	53	3.1×10^9	1050
Photek PMT Solar Blind	25.6	16.1	89	2.7×10^9	580
FBK SiPM w/UV Filter-I	17.8	14.7	62	2.4×10^9	800
Hamamatsu VUV MPPC	10.5	10.2	37	1.7×10^9	1120
SIC BaF_2:Y-2020					
Hamamatsu R2059 PMT	15.2	18.7	45	1.3×10^9	810
Photek PMT Solar Blind	25.6	16.1	76	1.1×10^9	450
FBK SiPM w/UV Filter-I	17.8	14.7	53	1.0×10^9	610
Hamamatsu VUV MPPC	10.5	10.2	31	7.1×10^8	870
BGRI BaF_2-1507					
Hamamatsu R2059 PMT	15.2	20.0	46	5.8×10^9	1650
Photek PMT Solar Blind	25.6	13.0	77	3.8×10^9	790
FBK SiPM w/UV Filter-I	17.8	13.5	54	3.9×10^9	1160
Hamamatsu VUV MPPC	10.5	9.9	32	2.9×10^9	1680
SIC BaF_2-2					
Hamamatsu R2059 PMT	15.2	20.0	48	5.8×10^9	1590
Photek PMT Solar Blind	25.6	13.0	81	3.8×10^9	760
FBK SiPM w/UV Filter-I	17.8	13.5	56	3.9×10^9	1120
Hamamatsu VUV MPPC	10.5	9.9	33	2.9×10^9	1620

4. Summary

- BaF_2 crystals provide ultrafast light with 0.5 ns decay time. Yttrium doping increases the F/S ratio while maintaining the ultrafast light intensity, promising an ultrafast calorimeter.
- RIN:ɣ was measured for two BaF_2:Y and three BaF_2 samples under 2 and 23 rad/h. 0.8 MeV RIN:ɣ is observed for BaF_2:Y samples as compared to 1.6 MeV for BaF_2 samples of 30×30×250 mm³ readout by R2059 PMT in 50 ns gate.
- RIN:ɣ is found to be highly correlated to the light output in 2.5 μs gate or the slow component. Both Yttrium doping and solar blind photodetector are required to further reduce the RIN:ɣ to < 0.6 MeV.
- ɣ-ray induced damage in BaF_2:Y crystals is sample dependent. R&D is needed for improvement. Measurements are on the way for both ɣ-rays and neutrons.

Acknowledgments:

Work supported in part by the U.S. Department of Energy under Grant DE-SC0011925

Contact : zhu@caltech.edu